# High-speed wavefront control using MEMS micromirrors

T. G. Bifano and J. B. Stewart, Boston University  [5895-27]

## Introduction

Various deformable mirrors for high-speed wavefront control have been demonstrated in recent years. In adaptive optics and point-to-point communication, these devices have been used to reshape the wavefront of a propagating beam to compensate for aberrations in the beam path.

An important, emerging class of deformable mirrors is those that are created using microelectromechanical systems (MEMS) fabrication tools. Such devices take advantage of silicon batch processing, high-quality thin films, and micrometer-scale lithographic patterning techniques to produce electrostatic actuator arrays that support a continuous or segmented mirror.

Such MEMS deformable mirrors offer inherent advantages in speed, compactness, and economy in comparison to their macroscale counterparts. Limitations include relatively low optical power handling capability.

In this paper, one type of segmented MEMS mirror is evaluated in detail, particularly with regard to its usable actuation bandwidth. In many emerging applications it is important to operate devices at control bandwidths well above 10kHz. In this paper it is demonstrated that careful design and environmental control can permit actuator bandwidths exceeding 100 kHz. Alternatively, it will be shown that viscous air damping can limit MEMS device bandwidth to less than 10 kHz.

## The device

Boston University's MEMS deformable mirrors (DMs), in both continuous and segmented architectures, have been described previously. These silicon-based devices have the potential to modulate spatial and temporal features of an optical wavefront, and have applications in imaging, beam-forming, and optical communication systems. Techniques to improve the manufacturing, quality, and capability of these mirrors have been developed over the past decade. These mirrors, deformed using electrostatically actuated surface-normal actuators, have apertures ranging from 1 mm to 10 mm (corresponding to array sizes from 32 to 1024 actuators), maximum stroke ranging from 1.5 μm to 4 μm (depending on design), position repeatability better than 2 nm, no actuation hysteresis, surface flatness typically below 25 nm RMS, and reflectivity >80% in visible and near infrared wavelengths (with gold, silver, or aluminum coatings). The array consumes almost no power because of the small capacitance (~100 fF) of each actuator. Figure 1 shows a cross-sectional schematic of three actuators in a

segmented device. Figure 2 is a photograph of the 1024 actuator device in a test fixture.
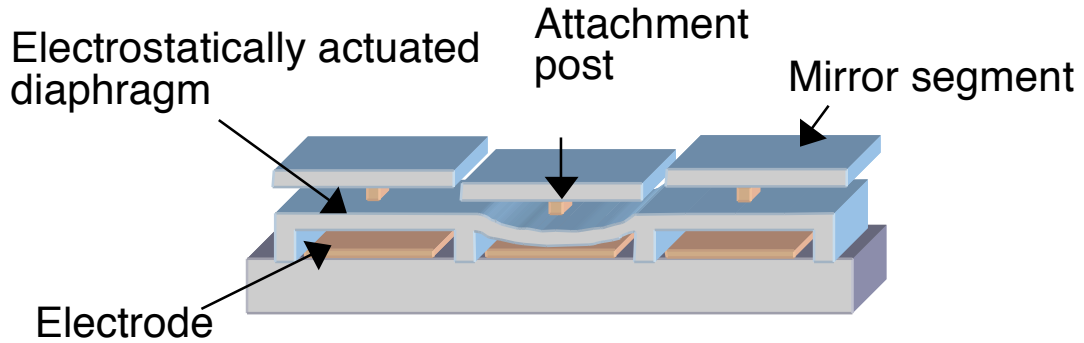


Figure 1: Cross sectional schematic of segmented MEMS DM showing three actuators.
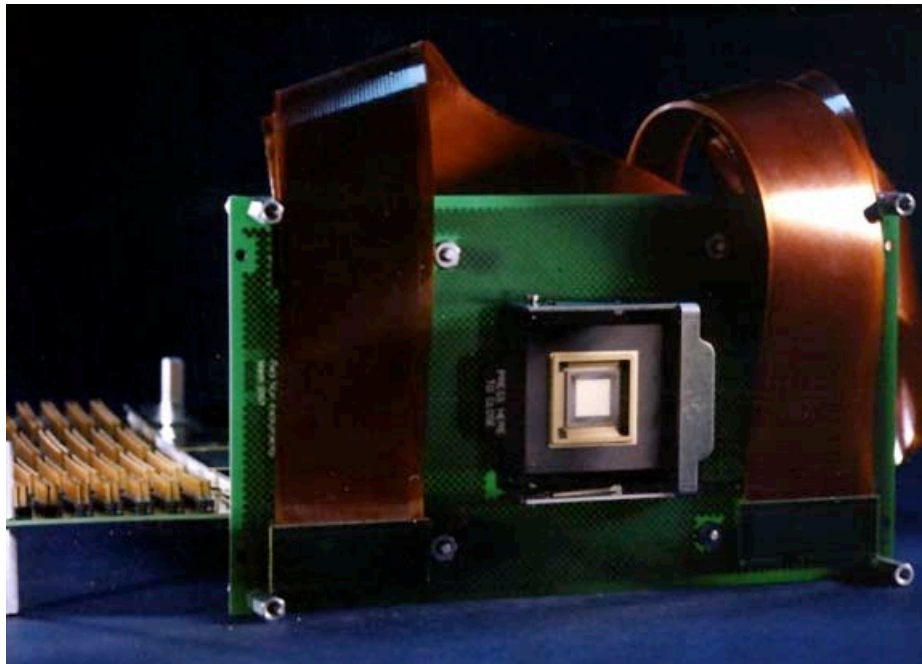


Figure 2: 1024 actuator segmented MEMS DM in a 32 x 32 array format. The central light square, measuring 10 mm across, contains the segmented mirror array. Also shown in the photo are the device ceramic package and an electronic testing board.

The DM has been characterized extensively and used in various wavefront control experiments. Figure 3 shows a measured surface contour of a portion of

the mirror array obtained using an interferometric surface-mapping microscope. One actuator is energized, causing a corresponding deflection of its mirror segment. Figure 4 shows the measured voltage vs. deflection behavior for one segment in two different DMs, illustrating good repeatability and nanometer-scale resolution.
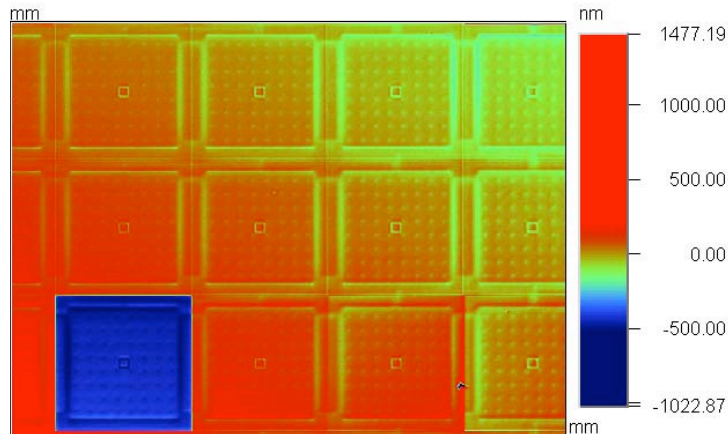


Figure 3: Surface map of a portion of the segmented MEMS DM, showing measured deflection of about 1 µm. The segment is approximately 300 µm square.
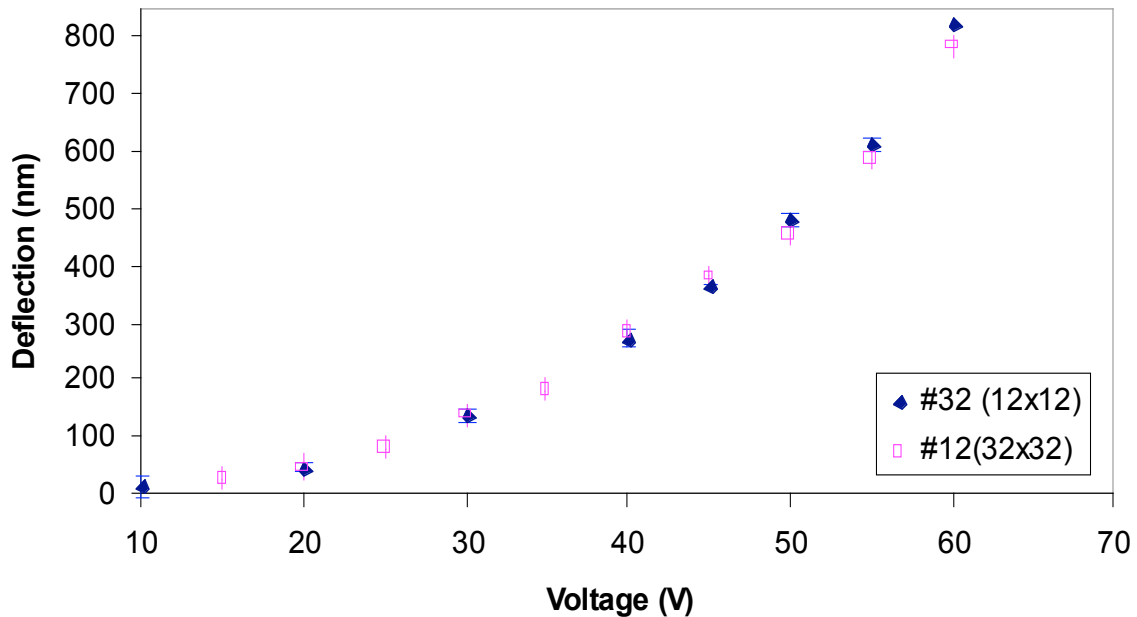


Figure 4: Measured voltage vs. deflection behavior for actuators on two different devices. The relationship is nonlinear, repeatable, and free of hysteresis.

**Device bandwidth**

Each segment of the DM is supported by a single electrostatic actuator, which is comprised of a compliant electrode diaphragm supported along two edges above a fixed electrode. The mirror segment is attached to the compliant diaphragm by a single post. A simplified mechanical analysis can be performed if it is assumed that the compliant actuator membrane acts like a beam fixed at both ends and the mirror acts as a concentrated load at the beam center. With these simplifications the actuator's natural frequency can be calculated from the geometric properties of the device and the mechanical properties of the silicon material. Since the mirror segment itself contains most of the moving mass during vibration, a first-order estimate of the natural frequency neglects the mass of the actuator:

$$f_n = \frac{1}{2\pi} \sqrt{\frac{192EI}{mL^3}}$$

where $f_n$ is the system resonant natural frequency, E is the elastic modulus of the actuator material (170 GPa for silicon), I is the compliant actuator diaphragm's bending moment of inertia, ($bh^3/12$, where b is the actuator width, 250 μm, and h is the actuator diaphragm thickness, 2 μm), and m is the mass of the mirror (its width, 300 μm, times its length L, 300 μm, times its thickness, 3 μm times its weight density, 23 kN/m$^3$). Using these values, one can estimate the actuator natural frequency to be approximately 40 kHz. A finite element numerical analysis of the system with the same parameters yields a resonant frequency of about 60 kHz.

When operating in air at standard pressure, the actuator's dynamics are affected by a phenomenon known as "squeeze-film damping." When the actuator is energized, the gap between the two electrodes narrows, forcing air out of the space between the electrodes. As air leaves the cavity, energy is dissipated through viscous drag at the actuator surface. This dissipation effect is rate dependent and can limit the usable actuation bandwidth of a MEMS DM.

To illustrate this effect, the surface-normal motion of a mirror segment was measured using a laser vibrometer while the corresponding electrostatic actuator was subjected to a step change in voltage equivalent to a steady-state displacement of 300 nm. The dynamic response of the segment was measured at standard atmospheric pressure (760 Torr) and then repeated after the MEMS device was sealed in an evacuated chamber (at 6 Torr) to eliminate the effect of air damping. Figure 5 shows the measured step-response for one mirror segment in air and vacuum. The lateral extent of the laser vibrometer measurement beam was about 30 μm, and the beam was centered on the 300 μm square segment during all measurements.

**Segmented mirror step response in air**
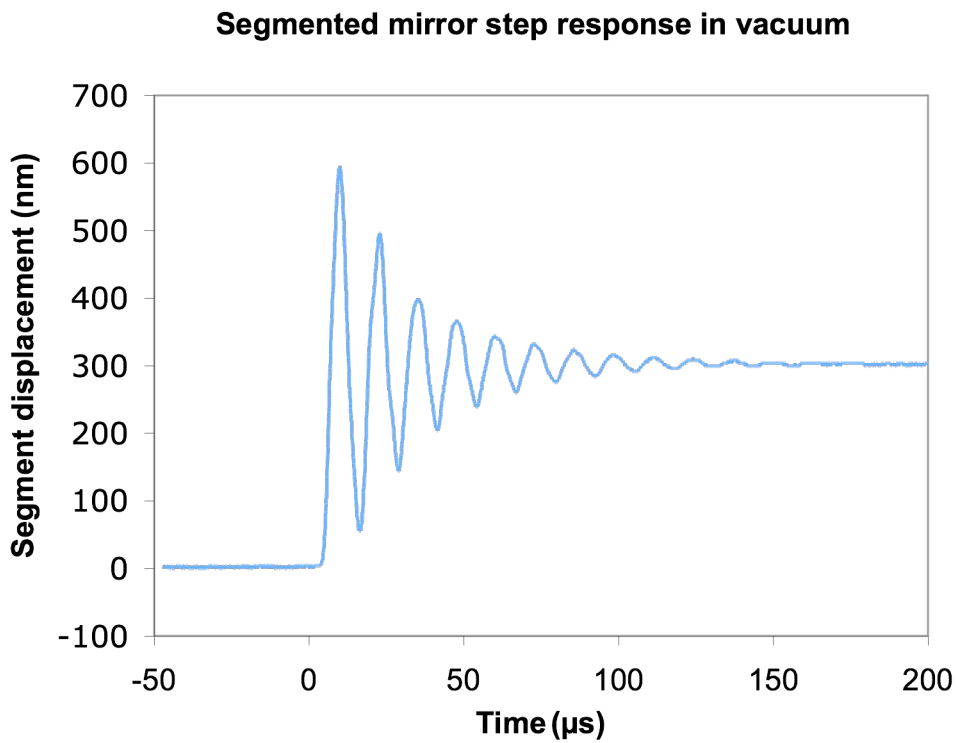
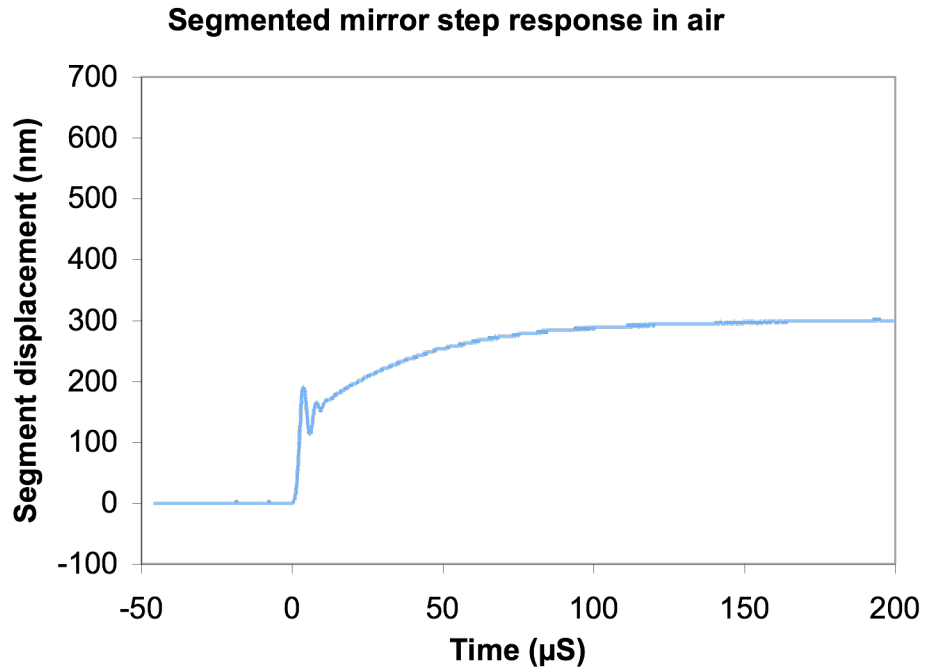**Segmented mirror step response in vacuum**

Figure 5: Measured step response in air and in vacuum for a MEMS DM segment. In air, the segment begins to move quickly after the step input, but viscous squeeze film effects damp its motion as air rushes out of the actuator gap. The total rise time to reach 95% of steady state is about 100 µs. In vacuum, the displacement of the segment exhibits damped oscillation about the

equilibrium position. Intrinsic material damping allows the oscillation to decay to within 5% of the equilibrium value in about 100 µs.

With 100 µs settling time, the segmented mirror device studied here is not capable of wavefront control at bandwidths above 10 kHz.  In the remainder of this document, we introduce three alternative ways to increase the bandwidth of this device by reducing its settling time. These three approaches to reducing actuator response time, which all proved successful, are:

- Controlling the environmental pressure
- Modifying the step input signal characteristics (*Two-step*)
- Restricting squeeze-film flow paths

## Controlling the environmental pressure

The first method to reduce actuator response time employed environmental pressure control, where the surrounding device pressure was varied to yield a compromise between over-damped behavior at atmospheric pressure and under-damped behavior in vacuum.

To illustrate the controllability of the relationship between environmental pressure and mirror dynamic response, measurements were made on mirror segments driven by an input signal consisting of a fixed DC offset (100 V) added to small (3 V) sinusoidal signal that was slowly swept in a frequency range from 100 Hz to 100 kHz. These measurements were repeated for several different environmental conditions, as noted in the legend in Figure 6. Because the actuator's deflection is a nonlinear function of voltage, the physical relevance of such a Bode diagram is limited to small signal inputs near this particular offset. However, the results can be used to demonstrate the device response qualitatively and to gauge the effect of partial pressure on damping.

It is seen from this data that in air at atmospheric pressure (760 Torr), the response amplitude declines steadily for frequencies >5 kHz, illustrating significant over-damping. Conversely, at the lowest pressure used in this experiment (6 Torr), there is no such decline at higher frequencies, but there is a sharp peak at about 60 kHz, corresponding to the under-damped response that was detailed in Figure 5. At intermediate pressures the frequency response curves flatten over the measurement bandwidth. The optimum behavior appears at about 250 Torr, for which the squeeze film damping effects are considerably reduced, and the resonant peak is nearly eliminated.

This approach has the merits of being relatively straightforward and passive. As long as the environment is controlled, the dynamic response will be modified accordingly. Nevertheless, packaging devices in partial vacuum is non-standard, and presents a considerable engineering challenge.
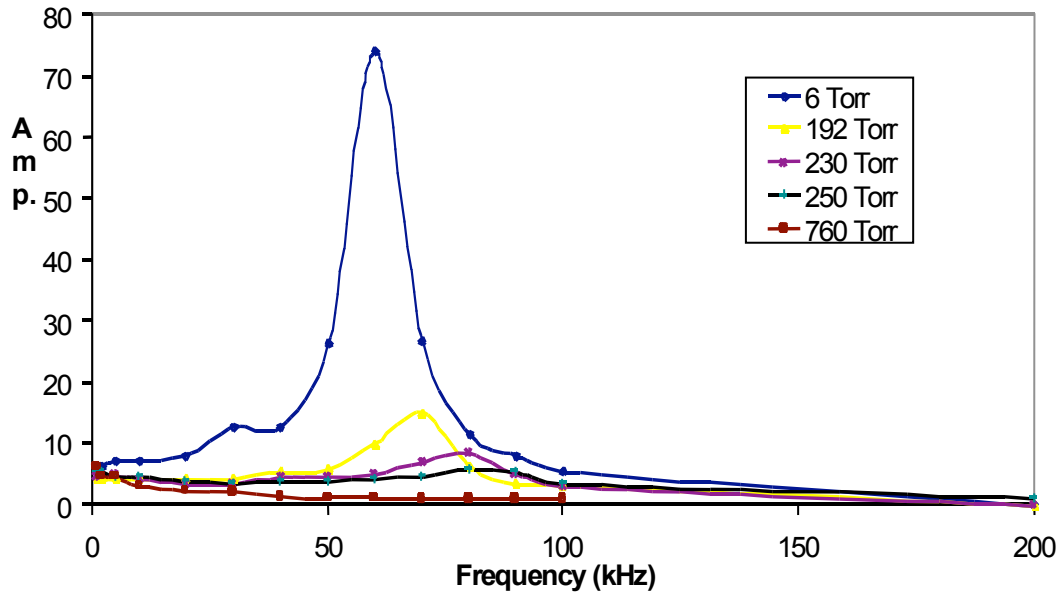
Figure 6: Measured small-signal frequency response for a segmented mirror actuator. The vertical axis scale is in arbitrary magnitude units.

**Modifying the step input signal characteristics (*Two-step*)**

A second approach to increasing step response characteristics of the device is one that takes advantage of the repeatable, well behaved, second-order oscillatory response observed in vacuum. This behavior is characteristic of an under-damped spring-mass-damper system, which has a solution to a step input from an initial state of rest of the form:

$$d(t) = A(1 - e^{-t/\tau} \cos \omega t)$$

where d is the segment displacement, A is the steady state displacement, $\tau$ is the oscillation decay time constant (physically the product of the damping ratio and the actuator natural frequency, or $\zeta \omega_n$), $\omega$ is the oscillation frequency (physically the product of the actuator natural frequency and a term related to damping coefficient $\omega_n \sqrt{[1-\zeta^2]}$), and t is the time measured from the input step change. The step-response data measured in vacuum (shown previously in Figure 5) closely follows this form.

This particular solution to the linear vibration problem obeys the rules of superposition, suggesting that one way to achieve a rapid response from the actuator is to drive it with a carefully sized and timed sequence of two step

inputs, coordinated so that the oscillations due to the first step are cancelled by the oscillations due to the second step.

Mathematically, the compound step input, I(t), follows the form:

$$I = C \cdot \begin{cases} \alpha & 0 \le t < \dfrac{\pi}{\omega} \\ 1 & \dfrac{\pi}{\omega} \le t \end{cases}$$

where C is the input step required to produce the desired steady-state displacement, A, and $\alpha$ is a fraction corresponding to the damping ratio ($\alpha = 1/2(1-\zeta\pi)$). In Figure 7, the concept is demonstrated through simulation of a system with damping ratio 0.15 and natural frequency of 36 kHz. At time t=0, the first step input is applied, corresponding to 61.5% of the total required step height. After about 17 µs the remainder of the step is applied, adding to the first step and canceling its oscillations. The combined response of the actuator in this simulation is such that the steady-state value is reached in 17 µs, a settling time more than five times faster than without the two-step approach.
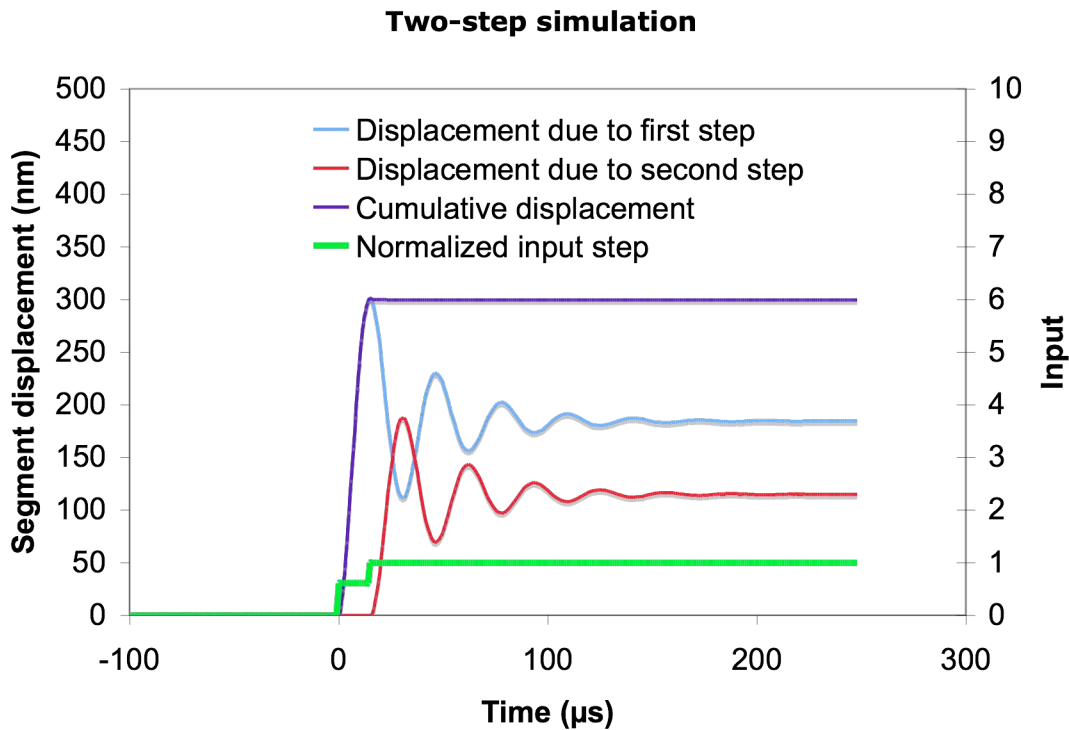
**Two-step simulation**



Figure 7: Simulated two-step control input used to decrease step response time by canceling oscillations due to under-damped behavior of the actuator in vacuum.

To demonstrate this principle on a real actuator, the device was first characterized by its single-step response curve as depicted in Figure 5. The best-fit parameters to the second order step response equation for that data correspond to values of A = 300 nm, τ = 40 μs, and ω = 0.5 rad/μs.  From this fit the two critical parameters were determined for the relative amplitude of required displacement steps (α = 0.54) and the time delay for the second step (π/ω~7.4 μs). (Also from this fit, the natural frequency and damping ratio for the actuator were determined to be $f_n$ = 81 kHz and ζ = 0.05). These parameters will work equally well for arbitrary displacement step sizes (C). However, it is important to note that the although relative amplitude of displacement steps remains fixed, the relative amplitude ratio of *voltage* steps does not remain fixed because displacement and voltage are related nonlinearly.  For the 300 nm step chosen to demonstrate this two-step algorithm, the α=0.54 relative displacement step height parameter suggests a first step of 54% of 300 nm and a second step of 46%. The corresponding requirement is for 78% of the overall voltage in the first step and the remaining 22% in the second step.

This ratio of voltage steps, with the requisite two-step delay, was applied to an actuator. Both the input voltage and the output response were measured and compared to the single-step data corresponding to the same steady-state displacement. The results are shown in Figure 8 (input) and Figure 9 (response).
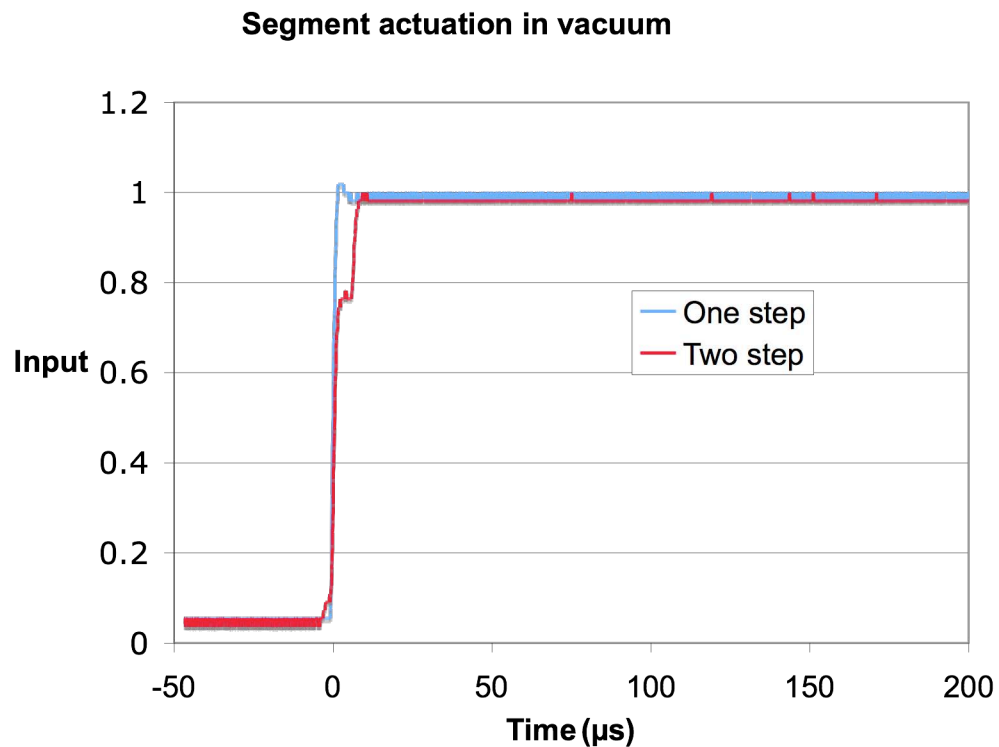


**Segment actuation in vacuum**

Figure 8: Measured input voltages used in comparison of one-step response and two-step response.
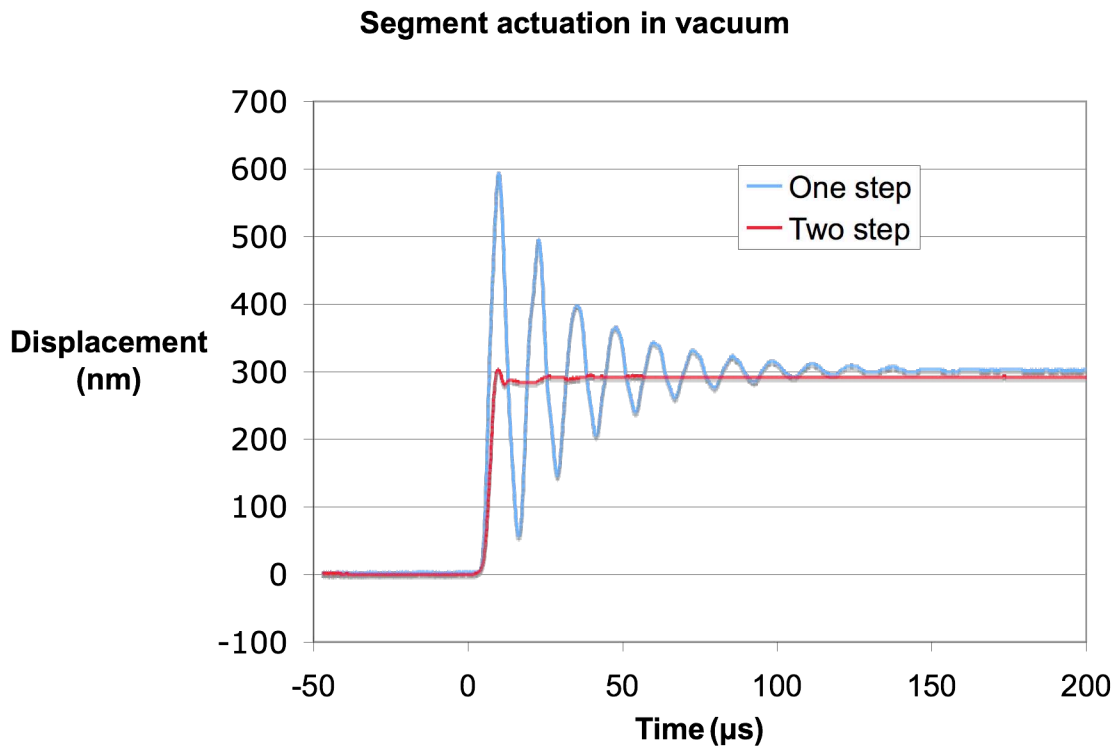
**Segment actuation in vacuum**



Figure 9: Comparison of measured one-step response and two-step response for a segmented mirror actuator. The two-step response permits significant reduction of settling time.

The two-step approach is fairly robust. Parameter variation of up to 10% of the measured values has relatively little effect on the response. However, this approach does require some extra sophistication in the driver, which needs to be able to provide precisely timed and scaled pairs of step outputs. Also, the technique requires vacuum packaging of the DM device.

## Restricting squeeze-film flow paths

One of the common design rules for MEMS fabrication is that each structural layer must have regularly spaced perforations (called etch access holes) to aid in rapid dissolution of the sacrificial layers of the device after deposition and patterning processes are completed. These etch access holes also provide paths for airflow during actuation of the device. No significant modeling of microfluidic flow responsible for squeeze-film damping of the devices described in this paper has been conducted. However, it is safe to say that the flow through the dozens of etch access holes in the actuator diaphragm contribute substantially to squeeze-film behavior.

A batch of devices was fabricated without etch access holes in the actuator diaphragm, and the damping behavior of those devices were compared to those

with etch access holes. The results showed dramatic decrease in settling time (i.e. faster response) for actuators that had no etch access hole in the actuator diaphragm. Figure 10 illustrates this effect through measured step response of two otherwise identical actuators in an environment of air at standard pressure. The device without etch access holes settles to within 5% its steady-state value in about 10 µs. This is comparable to the behavior achieved using the two-step approach, but has the advantage that the device does not need to be vacuum packaged and does not require complex control electronics.

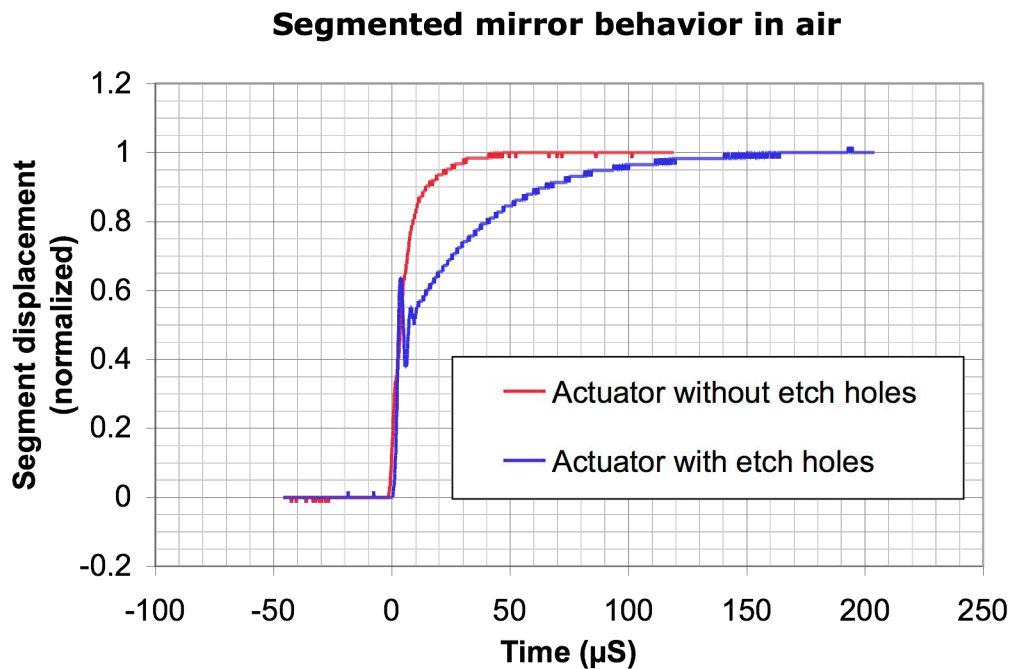## Segmented mirror behavior in air



Figure 10: Mirror segment step response in air for two identical devices, except that one (the faster one) has no etch access holes in the actuator diaphragm and the other does. The etch access holes contribute significantly to air damping, slowing the device response.

## Conclusions

Segmented MEMS deformable mirrors have the potential to modulate wavefront shape at frame rates of up to 100 kHz, though squeeze-film air damping limits that speed in practice by an order of magnitude to 10 kHz. Three distinct approaches to obtaining 100 kHz response have been described in this paper. All were tested successfully. The most promising of these is based on a manufacturing redesign to eliminate flow paths through the actuator diaphragm.